Talanta 81 (2010) 1162–1169

Contents lists available at ScienceDirect

Talanta

journal homepage: www.elsevier.com/locate/talanta

# Synthesis of magnetic and fluorescent bifunctional nanocomposites and their applications in detection of lung cancer cells in humans

Jingwei Ma[a], Qishi Fan[b], Lianhui Wang[c], Nengqin Jia[a], Zhidong Gu[b], Hebai Shen[a,*]

[a] Department of Chemistry, Life and Environment Science College, Shanghai Normal University, No. 100 Guilin Road, Shanghai 200234, PR China
[b] Department of Laboratory Medicine, Ruijin Hospital, Shanghai Jiaoton University School of Medicine, Shanghai 200025, PR China
[c] Laboratory of Advanced Materials, Fudan University, Shanghai 200433, PR China

ARTICLE INFO

*Article history:*
Received 19 August 2009
Received in revised form 18 January 2010
Accepted 20 January 2010
Available online 10 February 2010

*Keywords:*
Fluorescence
Magnetism
Bifunctional nanocomposites
Cancer cells detection
Quantum dots

ABSTRACT

We developed a novel strategy to detect lung cancer cells by utilizing magnetic and fluorescent bifunctional nanocomposites (BNPs) in combination with monoclonal anti-carcinoembryonic antigen (CEA) antibodies. The BNPs, consisting of silica-coated superparamagnetic nanoparticles and quantum dots (QDs), exhibited high luminescence and were easily separated in an external magnetic field. The binding specificity of the antibody-conjugated BNPs (immunonanoparticles) were confirmed via incubating with human lung adenocarcinoma SPCA-1 cells, human leukemic K562 cells and human embryonic lung fibroblasts MRC-5 cells. Further experiments demonstrated that the as-prepared immunonanoparticles can efficiently capture and detect cancer cells in pleural effusion from lung cancer patients. These results suggest that this method, of which the detection procedures are completed within 1 h, could be applied to the rapid and cost-effective monitoring of cancer cells in clinical samples.



## 1. Introduction

Lung cancer is one of the most life threatening cancer diseases and shows high incidences in both men and women worldwide. Approximately 75–80% of lung cancer patients suffer from non-small cell subtype which can be removed by surgery if detected in early stage. However, more than 80% of the patients are only diagnosed at time of advanced stage when therapeutic options are restricted to systemic chemo- and radiotherapy [1–3]. Therefore, early detection seems to be the key for lung cancer survival. Nowadays, some routine biochemical and histopathological assays and graphical methods including sputum cytology, chest radiograph, fluorescence bronchoscopy, polymerase chain reaction (PCR), computed tomography (CT) and bronchial biopsy have been widely used in lung cancer detection. However, ability to use these techniques is dependent on the size of tumor and some special medical equipment, leading to the cost escalation.

It is reported that the cancer marker expression on the cell membrane is useful in the diagnosis and clinical management of patients with lung cancer. That is because they can provide insight into histogenesis, interrelationships and biological behavior of lung tumors [4]. Also, there is increasing evidence that cancer marker can provide prognostic information in non-small cell lung cancer (NSCLC) [5–7]. According to Muley et al. [8], CEA and cytokeratin-19 fragments (CYFRA 21-1) proved to be sensitive and valuable biomarkers for estimation of diagnosis, prognosis and therapy monitoring in NSCLC. Accordingly, cancer marker used alone or in combination with other techniques may play an important role in monitoring NSCLC in early stage.

In the past decade, nanotechnology and nanomaterials have shown great potential in disease diagnosis and therapy [9,10], especially inorganic nanomaterials are increasing in their popularity in biomedical application. Much attention has been focused on nano-sized inorganic particles including magnetic nanoparticles and quantum dots (QDs) due to their unique optical, electrical and magnetic properties [11], which can be widely applied in disease diagnosis and therapy. Magnetic iron oxide nanoparticles have been extensively used as magnetic resonance imaging (MRI) contrast agents [12], drug delivery systems [13] and cell separation [14]. Semiconductor nanocrystals, commonly called quantum dots, have also shown significant potential for various applications ranging from QD lasers to biological tagging [15]. QDs have superior fluorescent properties and marked advantages over conventional fluorescent dyes, such as broad excitation, size-dependent photoluminescence with narrow emission bandwidth covering a wide spectral range, unusual photochemical stability and relatively high photoluminescent quantum yield [16,17]. All these make them ideal as a class of fluorescent

* Corresponding author. Tel.: +86 21 64321800; fax: +86 21 64321800.
*E-mail address:* shenhb@shnu.edu.cn (H. Shen).

0039-9140/$ – see front matter © 2010 Elsevier B.V. All rights reserved.
doi:10.1016/j.talanta.2010.01.042

probes used in biological system, especially in cellular imaging [18,19].

More recently, there have always been some needs for materials with the functions of both magnetic separation and fluorescent label in biomedical field [20]. The common strategy is to anchor magnetic nanoparticles and organic dyes or lanthanide metal complexes, respectively [21,22]. The method is complicated, time-consuming, and relatively inefficient [23]. Besides, QDs and magnetic nanoparticles can also simultaneously coated into a matrix [24]. But the distances of QDs and magnetic nanoparticles usually are too close to be controlled, causing a strong interaction between QDs and magnetic nanoparticles, which can decrease the photoluminescence dramatically [25]. Although magnetic and fluorescent nanocomposites have been investigated by some researchers, up to now there is little report on using such nanocomposites to detect lung cancer cells.

In this paper, a novel and rapid method has been put forward to simultaneously enrich and detect rare cancer cells by BNPs which can be controlled by an external magnetic field and monitored by their intense luminescence. We fabricated BNPs that incorporated magnetic nanoparticles in silica shell and water-soluble QDs immobilized on the silica surface. The BNPs demonstrated their targeting effect to capture SPCA-1 cells after surface-modification with anti-CEA antibodies. We then used these immunonanoparticles to separate and detect cancer cells in the pleural effusions from the patients. Confocal laser scanning microscopy (CLSM) was conducted to have a qualitative assessment of cellular targeting of immunonanoparticles. The process described above is depicted simply in Fig. 1. We believe that exploiting multifunctional nanocomposites could provide a more fantastic and sensitive candidate for cancer early detection.

## 2. Experimental

### 2.1. Materials

The 3-mercaptopropionic acid (MPA)-capped CdTe QDs (emission, 658 nm; diameter, 4 nm) were kindly provided by Prof. Lianhui Wang (Fudan University in China). The human lung adenocarcinoma cell line SPCA-1, human leukemic cell line K562 were purchased from the Cell bank of Chinese Academy of Sciences and the human embryonic lung fibroblasts cell line MRC-5 was a gift from Prof. Jianwen Liu (East China University of Science and Technology). 1-Ethyl-3-(3-dimethylaminopropyl) carbodiimides hydrochloride (EDAC) and N-(2-aminoethyl)-3-aminopropyltrimethoxysilane (AEAPS) were purchased from Sigma–Aldrich. RPMI-1640 was obtained from Sino-American Biotechnology Co. Ltd. Fetal bovine serum (FBS) was purchased from Shanghai Zhuokang Biotechnology Co. Ltd. Mouse monoclonal anti-CEA antibodies were obtained from Zymed Laboratories, Inc. All other reagents were of analytical grade. Double distilled water was used for all the experiments.

### 2.2. Synthesis of silica-coated superparamagnetic nanoparticles ($SiO_2/\gamma$-$Fe_2O_3$ MNPs)

The silica-coated superparamagnetic nanoparticles were prepared by our reported method [26]. Typically, 2.5 M NaOH solution was dropped into the solution of mixture of $FeCl_3$ (0.2 M) and $FeSO_4$ (0.12 M) with violently stirring. Then the obtained precipitation was aged at the temperature of 60 °C for 2 h and washed with water for several times. Finally, the magnetic nanoparticles were dried at 60 °C for 24 h. To coat the magnetic nanoparticles with silica, we adopted the water-in-oil reverse microemulsion of water/Triton X-100/n-hexylalcohol/cyclohexane. 0.1 g of $\gamma$-$Fe_2O_3$ was dispersed in the 60 ml above microemulsion with 3 min ultrasonication, then the solution was poured into three-necked flask with vigorous stirring at 22 °C. Concentrated ammonia and tetraethoxysilane were added dropwise into the system in turn. The reaction ended after 10 h. The nanoparticles were aged overnight and then washed with ethanol three times. At last, the $SiO_2/\gamma$-$Fe_2O_3$ MNPs were redispersed in ethanol and sonicated for 10 min to prevent aggregation.

### 2.3. Modification of $SiO_2/\gamma$-$Fe_2O_3$ MNPs with AEAPS [27]

Appropriate amount of $SiO_2/\gamma$-$Fe_2O_3$ MNPs was dispersed in the mixture of 25 ml methanol and 15 ml glycerol with 30 min ultrasonication. Then 0.5 ml AEAPS was added into the mixture and dispersed by vigorous stirring. Through the whole experiment, the temperature was retained at 60 °C. The amino-functionalized $SiO_2/\gamma$-$Fe_2O_3$ MNPs ($NH_2$–$SiO_2/\gamma$-$Fe_2O_3$ MNPs) were washed with ethanol and 0.01 M phosphate-buffered saline (PBS, pH 7.4) for three times, respectively. Finally the $NH_2$–$SiO_2/\gamma$-$Fe_2O_3$ MNPs were retained in PBS.

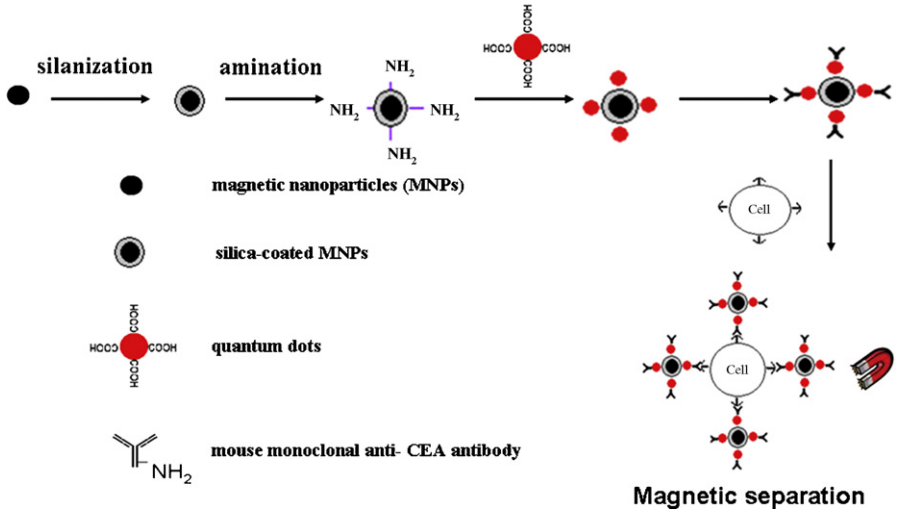


**Fig. 1.** Schematic illustrations of synthesis of magnetic and fluorescent bifunctional nanocomposites and they used for cancer cells capture and detection.

### 2.4. Preparation of magnetic and fluorescent nanocomposites (QDs-$SiO_2$/γ-$Fe_2O_3$ MNPs)

The MPA-capped CdTe QDs with emission maximum of 658 nm were used to attach $NH_2$–$SiO_2$/γ-$Fe_2O_3$ MNPs through EDAC coupling [28]. Briefly, 5 mg EDAC coupling reagent was added into 1 ml PBS containing 1.3 mM QDs. After incubation for 15 min, 1% (w/v) $NH_2$–$SiO_2$/γ-$Fe_2O_3$ MNPs suspension was also added. The mixture was then allowed to react for 2 h under gently shaken at room temperature. The BNPs were then collected by magnetic separation, followed by washing several times with PBS. Ultimately, the BNPs were redispersed in PBS for further characterization.

### 2.5. Preparation of antibody-conjugated QDs-$SiO_2$/γ-$Fe_2O_3$ MNPs

In order to investigate whether the BNPs can be used to capture rare cancer cells followed by luminescence detection or not, bioconjugation of the anti-CEA antibodies with BNPs also through EDAC coupling was prepared. The experimental details were described as follows. Firstly, BNPs were reacted with 5% (w/v) EDAC in PBS for 15 min and then an appropriate amount of anti-CEA antibodies was added. After 3 h, the antibody-conjugated BNPs (immunonanoparticles) were isolated from the mixture by a permanent magnet and washed several times with PBS.

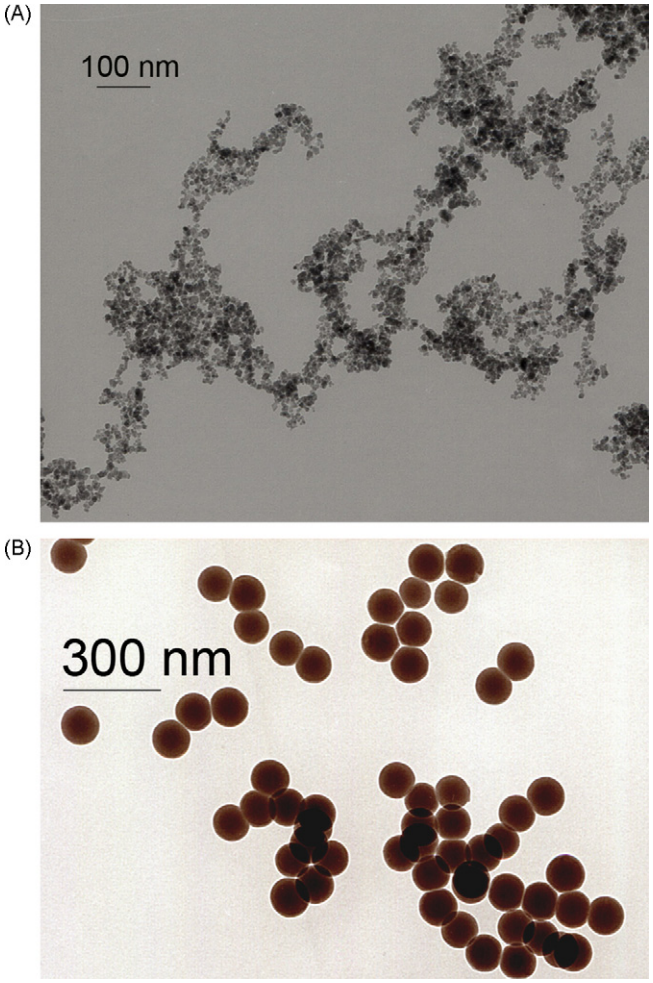


**Fig. 2.** TEM images of γ-$Fe_2O_3$ nanoparticles (A) and $SiO_2$/γ-$Fe_2O_3$ MNPs (B).

### 2.6. Cell culture and immunomagnetic separation–fluorescent detection of carcinoma cells

Human lung adenocarcinoma cell line SPCA-1, human leukemic cell line K562 and human embryonic lung fibroblasts cell line MRC-5 were routinely cultured at 37 °C in flasks containing RPMI-1640 medium, supplemented with 10% FBS in a humidified atmosphere with 5% $CO_2$. To perform target cells captured by the immunonanoparticles, SPCA-1 cells were detached using 0.25% trypsin–EDTA solution and then collected by centrifugation at 1000 rpm for 5 min. Subsequently, the cells were resuspended in PBS and the cells concentration was determined by hemocytometry. Immunonanoparticles were added and incubated for 45 min at ambient temperature. Afterwards, the cells were collected by magnetic separation, washed and photographed. As control experiments, pure BNPs were incubated with SPCA-1 cells and immunonanoparticles were incubated with CEA-negative K562 cells and MRC-5 cells under the same conditions, respectively.

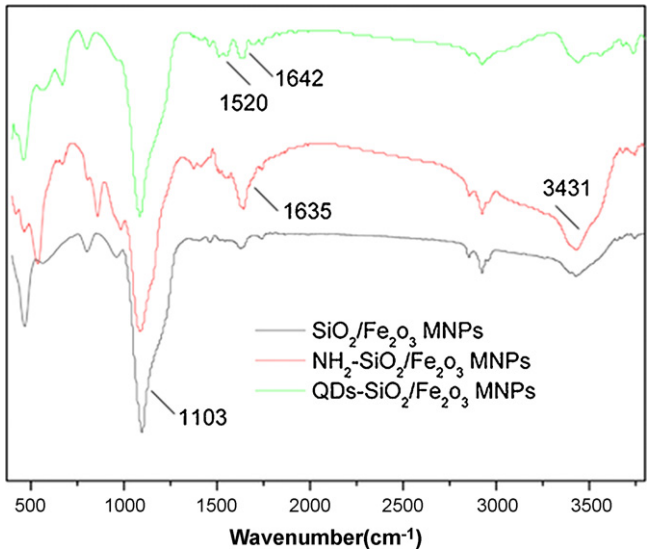


**Fig. 3.** FTIR spectra of $SiO_2$/γ-$Fe_2O_3$ MNPs, $NH_2$–$SiO_2$/γ-$Fe_2O_3$ MNPs and QDs-$SiO_2$/γ-$Fe_2O_3$ MNPs.

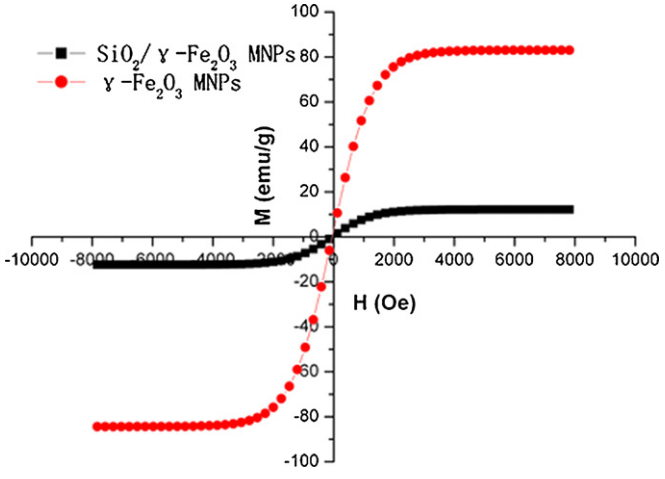


**Fig. 4.** Hysteresis loops for the γ-$Fe_2O_3$ nanoparticles and $SiO_2$/γ-$Fe_2O_3$ MNPs at room temperature.

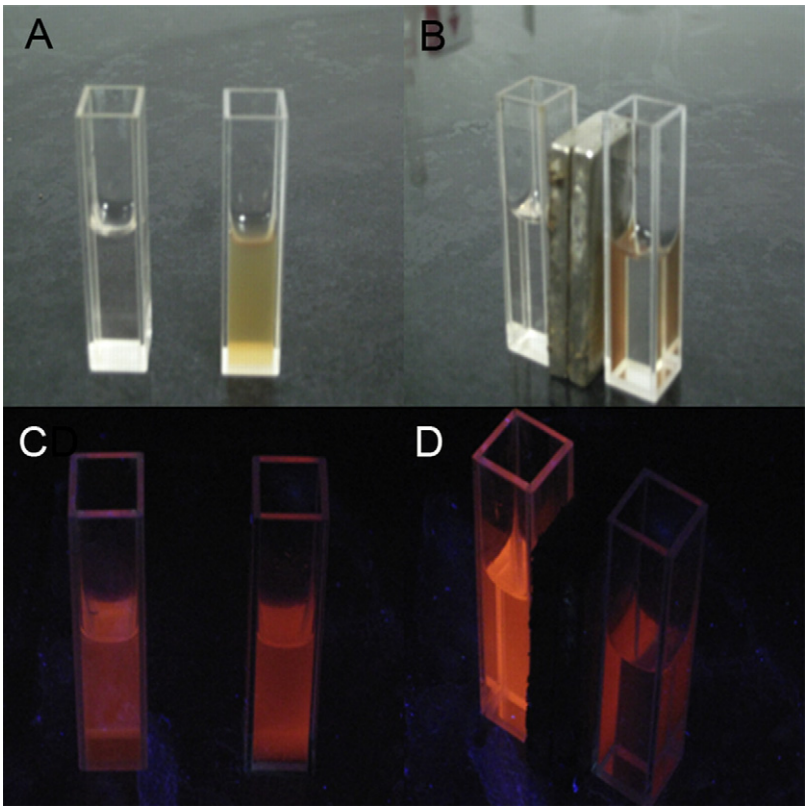


**Fig. 5.** Left column: photographs of pure QDs (left vial) and BNPs (right vial) under daylight (A) and UV light (C). Right column: the photographs were taken in daylight (B) and UV light (D) after a permanent magnet was fixed in between two vials.

### *2.7. Detection of carcinoma cells in pleural effusion by immunonanoparticles*

The benign and malignant pleural effusions of patients were obtained from Department of Laboratory Medicine, Ruijin Hospital of Shanghai Jiao Tong University in China. The study was approved by the Local Ethics Board, and informed consent was obtained from all patients. Ten patients with newly diagnosed lung cancer (8 male, 2 female) consisting of 5 adenocarcinomas, 3 squamous cell carcinomas and 2 small cell carcinomas were involved in this study. As control, 3 patients with tuberculous pleuritis (2 male, 1 female) were also entered. The age range was from 39 to 60 years, with a mean age of 52.5 years.

To enrich and detect cancer cells, we used 50 ml of fluid for each case and then 0.1 ml immunonanoparticles was added to the fluid samples. The samples were incubated at ambient temperature for 45 min with gentle shaken and were then placed in a magnet for 1 min. The supernatant was carefully removed by pipetting. The sample tubes were then removed from the magnet. Cells specifically bound to immunonanoparticles were selected by washing with PBS and were resuspended in 0.5 ml PBS. At the same time, all effusions were submitted for routine cytological examination in the usual manner.

### *2.8. Instruments and measurements*

The size and morphology of $SiO_2/\gamma$-$Fe_2O_3$ MNPs were measured on a HITACHI model H-600 transmission electron microscope (TEM). The FTIR spectra of the BNPs were obtained on a Thermo Nicolet 370 FTIR spectrophotometer. Pressed pellets were prepared by grinding the powder specimens with KBr in an agate mortar. The spectra were scanned from 4000 to 400 $cm^{-1}$. The magnetic property of BNPs was measured on a JDM-13 vibrating sample magnetometer. Ultraviolet–visible (UV–vis) absorption spectra of pure antibodies and immunonanoparticles were taken on a Varian Cary 100 UV/Vis Spectrophotometer. Also, the photoluminescence (PL) spectra excited at 250 nm were acquired by using a Varian Cary Eclipse Fluorescence Spectrophotometer, with samples dispersed in PBS. The fluorescent images of the cells with 488 nm excitation were carried out on a Zeiss LSM 510 META confocal laser scanning microscope.

## 3. Results and discussion

The basic scheme of our strategy for rapid capture and detection of cancer cells are shown in Fig. 1. In this scheme, the BNPs are used to conveniently attach the monoclonal antibodies that are specific for the target cells and after the cancer cells are captured by the immunonanoparticles, a magnetic field will be applied to isolate these immunonanoparticles and then red-emitting QDs probe deposited on silica surface can be used to monitor the cells.

Magnetic iron oxide nanoparticles have hydrophobic surfaces with a high surface-to-volume ratio, in the absence of any surface coating. Due to hydrophobic interactions between the nanoparticles, these nanoparticles agglomerate and form large clusters, resulting in increased nanoparticle size. When two large-particle clusters approach one another, each of them comes into the magnetic field of the neighbour. Since nanoparticles are attracted magnetically, surface-modification is often indispensable. In our work, the $\gamma$-$Fe_2O_3$ nanoparticles were coated with silica. These coatings provide not only stability to the nanoparticles in solution but also help in binding the various biological ligands at the nanoparticle surface for various biomedical applications. The TEM method was taken to characterize the coating result. Typical TEM images of the $\gamma$-$Fe_2O_3$ nanoparticles before and after coating with silica are shown in Fig. 2. Compared with Fig. 1A, Fig. 1B shows

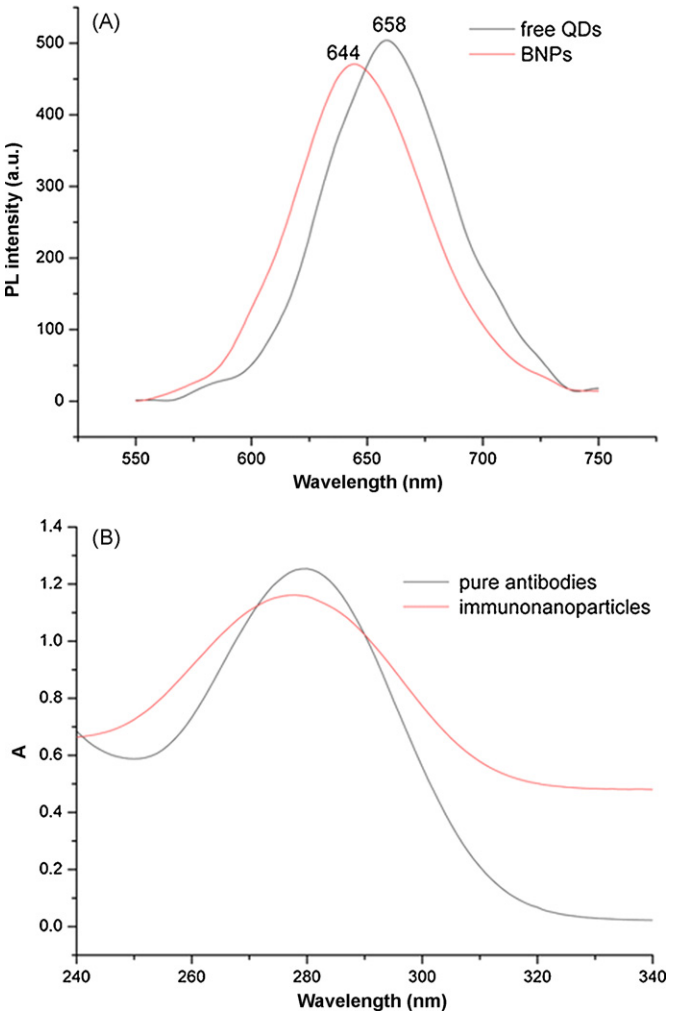


**Fig. 6.** PL spectra of free CdTe QDs and BNPs (A) and absorption spectra of the anti-CEA antibodies and antibody-conjugated BNPs (B).

that the coated particles were fairly monodisperse and spherical in shape and the average diameter of the particles was about 100 nm.

In our work, the $SiO_2/\gamma$-$Fe_2O_3$ MNPs were then coupled with CdTe QDs in order to form BNPs with superparamagnetic and luminescent functionalities. The FTIR method was applied to characterize the conjugation. Fig. 3 gives the FTIR spectra of $SiO_2/\gamma$-$Fe_2O_3$ MNPs, $NH_2$–$SiO_2/\gamma$-$Fe_2O_3$ MNPs and QDs-$SiO_2/\gamma$-$Fe_2O_3$ MNPs. From Fig. 3, the strong and wide absorption band at 1103 $cm^{-1}$ occurred in all three different spectra is due to the asymmetry stretching vibration of Si–O bond [13]. Compared with the spectrum of $SiO_2/\gamma$-$Fe_2O_3$ MNPs, $NH_2$–$SiO_2/\gamma$-$Fe_2O_3$ MNPs possessed the adsorption band at 3431 $cm^{-1}$ due to the stretching vibration of N–H bond, and at 1635 $cm^{-1}$ attributed to the bending vibration of the N–H bond [26]. After the amino groups were modified on the nanoparticles surface by silanization, the QDs were coupled with $NH_2$–$SiO_2/\gamma$-$Fe_2O_3$ MNPs through EDAC coupling. From the spectrum of QDs-$SiO_2/\gamma$-$Fe_2O_3$ MNPs, two new bands at about 1520 and 1642 $cm^{-1}$ appeared, corresponding to the amides I and II [29], suggesting the carboxyl groups of QDs have been covalently attached to amino groups on the silica surface.

Fig. 4 shows magnetic properties of free $\gamma$-$Fe_2O_3$ nanoparticles and BNPs. Both the $\gamma$-$Fe_2O_3$ nanoparticles and the BNPs exhibited the superparamagnetic characteristics. The saturation magnetization value of BNPs was 10.8 emu $g^{-1}$, which was much lower than that of $\gamma$-$Fe_2O_3$ nanoparticles (83.2 emu $g^{-1}$). The decreased magnetism may be attributed to the thick silica shell coated on magnetic nanoparticles. Nonetheless, the BNPs can still be enough for common bioseparation.

Because of the magnetic nanoparticles incorporated into silica shell, the BNPs can be directed to specific locations when manipulated by an external magnetic field, which, in this case, can be easily monitored through the intense luminescence of BNPs. Fig. 5 shows a series of photographs of an aqueous dispersion of BNPs and free QDs under UV light and daylight. While in the absence of an external magnetic field, the stable and monodisperse QDs (left vial) and BNPs (right vial) can be seen under daylight (Fig. 5A) and meanwhile the bright red fluorescence emitted from QDs and BNPs can also be observed from the whole dispersion (Fig. 5C). When an external magnetic field was placed between the two glass vials, only the BNPs were assembled to the side of the magnet within 30 s (Fig. 5B) and at the same time, a color change from the red to transparent was observed under UV light (Fig. 5D), demonstrating that the BNPs possessed strong magnetic property and with removal of the magnetic field followed by stirring, the aggregations were rapidly redispersed. Moreover these photographs further confirmed that QDs have been successfully immobilized on the silica shell and were not free in solution. The strong magnetism of BNPs, under an external magnet, could be applied to rapidly enrich rare cancer cells in clinical samples for cancer early detection.

The PL spectra of QDs and BNPs are shown in Fig. 6A. After coupled with QDs, the emission peak of BNPs shifted from 658 to 644 nm, showed a slight blue shift, and became less pronounced. But the peak still remained symmetry and narrow spectral width. The blue shift phenomenon has been observed previously for QDs immobilized on the surface of silica shell [30]. Then, in order to explore potential applications of BNPs in biomedical field, anti-CEA antibodies were conjugated with the BNPs through a coupling reaction between the carboxylic residues of MPA and amino groups of antibodies using EDAC. The use of EDAC coupling enabled the covalent attachment of the antibodies to the BNPs without substantially damaging the active site of the antibodies. Fig. 6B shows the absorption spectra of antibodies before and after attaching BNPs. It is known that the absorption peak of pure antibodies can be observed at around 280 nm. From the Fig. 6B, the absorption spectra of immunonanoparticles showed a pronounced peak corresponding to pure antibodies, indicating that the bioconjugate between BNPs and antibodies has been successfully formed.

To demonstrate the separation capability of the immunonanoparticles, we incubated a sample of 0.1 ml immunonanoparticles with a 3 ml SPCA-1 lung cancer cells suspension containing 10,000 cells/ml. Following 45 min incubation at room temperature, the cells were separated from the suspension using a permanent magnet. We further performed confocal fluorescence microscopy to observe the cells. The binding activity of immunonanoparticles to the SPCA-1 cells is shown in Fig. 7A. It can be observed that lots of cancer cells were separated from the suspension using a permanent magnet and apparent red fluorescence of immunonanoparticles was emitted from the cells surface, which proved that antigens have been recognized by the antibodies on the immunonanoparticles. Furthermore, almost one-to-one correspondence between cells shown in both bright field and dark field not only exhibits that the immunonanoparticles were still optically and biologically active, but also illustrates the availability of utilizing this strategy in lung cancer cells detection. In parallel, three control experiments were performed to further confirm the specificity and selectivity of immunonanoparticles under same conditions. First, little fluorescence sign was observed on the SPCA-1 cells after incubated with free BNPs (Fig. 7B). It is quite obvious that BNPs have negligible nonspecific interaction with cancer cells by comparison with immunonanoparticles. This phenomenon is likely due to lots of carboxylic groups with excess negative charges on the surfaces of QDs. Secondly,

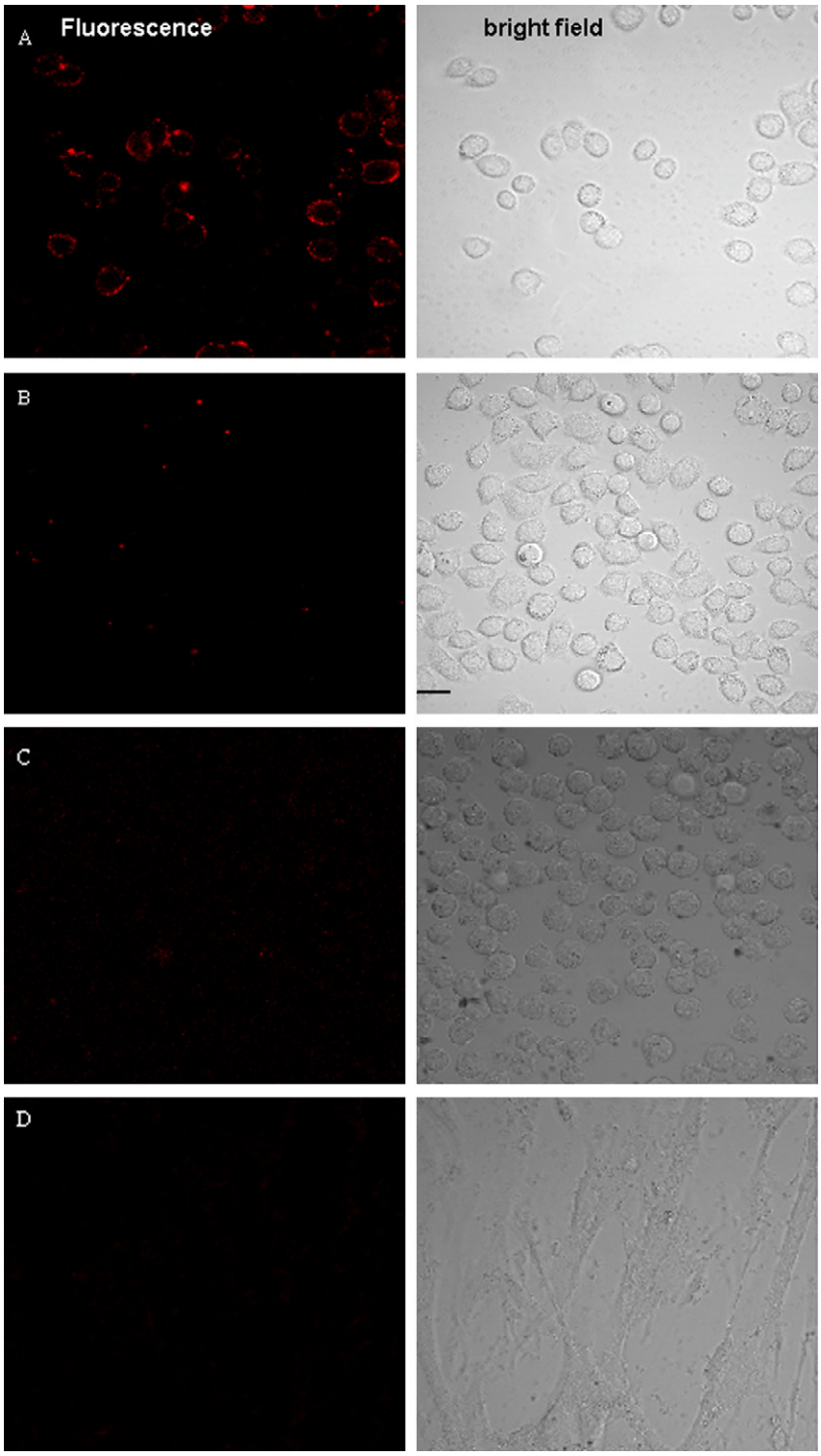


**Fig. 7.** Confocal microscopy images of SPCA-1 cells treated with immunonanoparticles (A), SPCA-1 cells treated with BNPs (B), K562 cells treated with immunonanoparticles (C) and MRC-5 cells treated with immunonanoparticles (D). Left column: fluorescence, right column: bright field. The scale bar corresponds to 20 μm.

immunonanoparticles were incubated with CEA-negative K562 cells (Fig. 7C). This experiment found nearly no fluorescence sign cannot be monitored, which confirmed that the successful targeting of immunonanoparticles to cells which express CEA. Thirdly, immunonanoparticles were treated with MRC-5 cells that is a type of CEA-deficient normal human lung cell (Fig. 7D). We found there was only a low level of nonspecific binding of immunonanoparticles to the normal human lung cell. In summary, these results of cells uptake present strong evidences about the targeting effect of immunonanoparticles for SPCA-1 cells.

Finally, to evaluate the feasibility of our strategy to detect cancer cells in clinical samples, we incubated immunonanoparticles with pleural effusions from patients and meanwhile, these samples were analyzed in parallel by cytological examination. Fig. 8 gives the representative images of CLSM obtained from pleural effusions of patients with lung cancer. As shown in the images, flu-

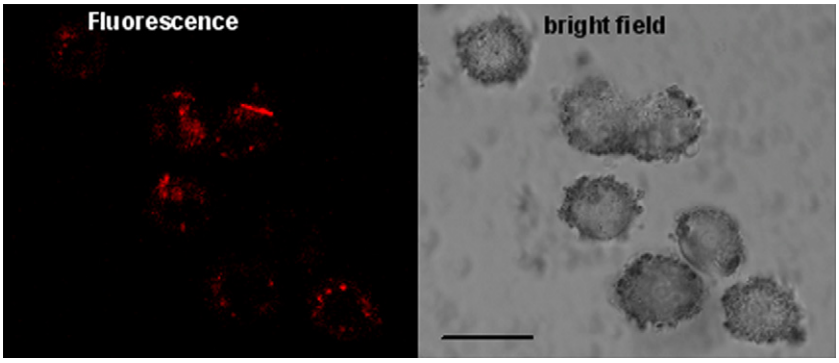


**Fig. 8.** Confocal microscopy images of cancer cells separated and detected by the immunonanoparticles in pleural effusion from a lung cancer patient. Left column: fluorescence, right column: bright field. The scale bar corresponds to 20 μm.

**Table 1**
Summary of results by immunonanoparticles detection and cytologic diagnosis.

| Samples | Method | Positive for malignancy | Negative for malignancy |
|---|---|---|---|
| Malignant pleural effusion | Immunonanoparticles detection | 7 | 3 |
| | Cytologic diagnosis | 6 | 4 |
| Benign pleural effusion | Immunonanoparticles detection | 0 | 3 |
| | Cytologic diagnosis | 0 | 3 |

orescence sign was clearly visible on the surface of cells, indicating the determination of the CEA on the cells surface.

Table 1 summarizes the results of studying 3 controls and 10 patients with lung cancer. Based on the results, cancer cells were found in 7 of 10 cancer patients and were not detected in control individuals, when examined by immunonanoparticles. On the other hand, 6 of 10 cancer patients were cytologically diagnosed to be positive for lung cancer and all patients with tuberculous pleuritis were negative. Overall, using immunonanoparticles to capture and detect cancer cells produced 70% sensitivity and 100% specificity in pleural effusion samples in comparison with 60% and 100% examined by cytology, respectively. Therefore, our presented immunonanoparticles detection assay has similar selection efficiency as compared with routine cytological examination.

Centrifugation has been widely used as a conventional method in cytological examination for preparing samples. However, it is tedious and of low yield, with poor quality of separation [31]. For example, discontinuous density gradient centrifugation only results in a 1.2- to 2.4-fold enrichment of bronchial epithelial cells from patients with lung cancer compared with a 36-fold enrichment by using magnetic cell separation [32,33]. In addition, because of the low percentage of cancer cells in clinical samples, many cytocentrifuge slides are needed to have enough cancer cells to be analyzed, making cytology very labor-intensive and time-consuming.

Immunonanoparticles detection assay, which the entire procedure can be completed within 1 h, could reduce labor and time consumption by using a simple process, and thus allow rapid analysis of clinical samples, particularly screening populations at high risk for lung cancer. More importantly, it is not limited by the need for complicated and expensive instruments and dedicated trained staff to operate the system, implying that our strategy is a relatively inexpensive procedure that could easily be available and accessible in many clinical settings.

The cancer cells detection studies described here made use of a single antibody and QDs of a single emission color. We assume the use of BNPs with different emission colors and different antibodies will enable the determination of multiple antigens on the cancer cells surface, which could significantly increase the specificity of cancer diagnosis at early stage. The detection capabilities of the different antibodies-conjugated BNPs of different emission colors in cancer cells suspensions are currently under investigation.

## 4. Conclusions

In summary, we reported a combined magnetic enrichment and optical detection strategy for lung cancer cells detection. The BNPs have excellent fluorescence, magnetism and conveniently conjugate with monoclonal anti-CEA antibodies, which can be used to recognize specifically SPCA-1 cells within a very short time. We envision the results by performing different control experiments that this method exhibits great potential to detect cancer cells in biological and biomedical applications, which are significantly benefit for cancer early diagnosis.

## Acknowledgements

This work was supported by Shanghai Science and Technology Committee (0752nm028, 08JC140600), the LADP-SHNU (DZL806), the National Basic Research Program of China (2008CB617504) and Shanghai Key Laboratory of Rare-earth Functional Materials (07dz22303).

## References

[1] A. Jemal, R. Siegel, E. Ward, T. Murray, J. Xu, C. Smigal, CA Cancer J. Clin. 57 (2007) 43.
[2] I. Norihiko, H. Aeru, I. Kentaro, H. Hidetoshi, T. Masahiro, U. Jitsuo, K. Harubumi, Lung Cancer 56 (2007) 295.
[3] S. Holdenrieder, J.V. Pawel, E. Dankelmann, T. Duell, B. Faderl, A. Markus, M. Siakavara, H. Wagner, K. Feldmann, H. Hoffmann, H. Raith, D. Nagel, P. Stieber, Lung Cancer 63 (2009) 128.
[4] J. Schneider, Adv. Clin. Chem. 42 (2006) 1.
[5] K. Suzuki, K. Nagai, J. Yoshida, E. Moriyama, M. Nishimura, K. Takahashi, Y. Nishiwaki, Ann. Thorac. Surg. 67 (1999) 927.
[6] J.L. Pujol, O. Molinier, W. Ebert, J.P. Daurès, F. Barlesi, G. Buccheri, M. Paesmans, E. Quoix, D. Moro-Sibilot, M. Szturmowicz, J.M. Bréchot, T. Muley, J. Grenier, Br. J. Cancer 90 (2004) 2097.
[7] T. Muley, H. Dienemann, W. Ebert, Anticancer Res. 23 (2003) 4085.
[8] T. Muley, T. Fetz, H. Dienemann, H. Hoffmann, F.J.F. Herth, M. Meister, W. Ebert, Lung Cancer 60 (2008) 408.
[9] L. Li, D. Chen, Y. Zhang, Z. Deng, X. Ren, X. Meng, F. Tang, J. Ren, L. Zhang, Nanotechnology 18 (2007) 405102.
[10] N. Jia, Q. Lian, H. Shen, C. Wang, X. Li, Z. Yang, Nano Lett. 7 (2007) 2976.
[11] V.L. Colvin, M.C. Schlamp, A.P. Alivisatos, Nature 370 (1994) 354.

[12] B. Feng, R.Y. Hong, L.S. Wang, L. Guo, H.Z. Li, J. Ding, Y. Zheng, D.G. Wei, Colloid Surf. A 328 (2008) 52.
[13] J. Zhang, R.D.K. Misra, Acta Biomater. 3 (2007) 838.
[14] W. Chen, H. Shen, X. Li, N. Jia, J. Xu, Appl. Surf. Sci. 253 (2006) 1762.
[15] R. He, X. You, J. Shao, F. Gao, B. Pan, D. Cui, Nanotechnology 18 (2007) 315601.
[16] A.P. Alivisatos, Science 289 (2000) 736.
[17] J. Weng, X. Song, L. Lia, H. Qian, K. Chen, X. Xu, C. Cao, J. Ren, Talanta 70 (2006) 397.
[18] Y. Shan, L. Wang, Y. Shi, H. Zhang, H. Li, H. Liu, B. Yang, T. Li, X. Fang, W. Li, Talanta 75 (2008) 1008.
[19] G. Yordanov, M. Simeonova, R. Alexandrova, H. Yoshimura, C. Dushkin, Colloid Surf. A 339 (2009) 199.
[20] H.Y. Xie, M. Xie, Z.L. Zhang, Y.M. Long, X. Liu, M.L. Tang, D.W. Pang, Z. Tan, C. Dickinson, W. Zhou, Bioconj. Chem. 18 (2007) 1749.
[21] T.J. Yoon, J.S. Kim, B.G. Kim, K.N. Yu, M.H. Cho, J.K. Lee, Angew. Chem. Int. Ed. 44 (2005) 1068.
[22] G.M. Qiu, Y.Y. Xu, B.K. Zhu, G.L. Oiu, Biomacromolecules 6 (2005) 1041.
[23] L.A. Perrin-Cocon, S. Chesne, I. Pignot-Paintrand, P.N. Marche, C.L. Villiers, J. Magn. Magn. Mater. 225 (2001) 161.
[24] D.K. Yi, S.T. Selvan, S.S. Lee, G.C. Papaefthymiou, D. Kundaliya, J.Y. Ying, J. Am. Chem. Soc. 127 (2005) 4990.
[25] X. Hong, J. Li, M. Wang, J. Xu, W. Guo, J. Li, Y. Bai, T. Li, Chem. Mater. 16 (2004) 4022.
[26] H. Shen, Y. Wang, H. Yang, J. Jiang, Chin. Sci. Bull. 48 (2003) 2698.
[27] X. Liu, J. Xing, Y. Guan, G. Shan, H. Liu, Colloid Surf. A 238 (2004) 127.
[28] S. Akyuz, T. Akyuz, Vib. Spectrosc. 42 (2006) 387.
[29] T. Aewsiri, S. Benjakul, W. Visessanguan, Food Chem. 115 (2009) 243.
[30] D. Wang, J. He, N. Rosenzweig, Z. Rosenzweig, Nano Lett. 4 (2004) 409.
[31] Q. Qiu, N.W. Todd, R. Li, H. Peng, Z. Liu, H.G. Yfantis, R.L. Katz, S.A. Stass, F. Jiang, Cancer 114 (2008) 275.
[32] C.D. Albright, J.K. Frost, N.J. Pressman, Cytometry 7 (1986) 536.
[33] S. Miltenyi, W. Muller, W. Weichel, Cytometry 11 (1990) 231.